Sharkskin and Oscillating Melt Fracture: Why in Slit and Capillary Dies and Not in Annular Dies?

O. Delgadillo-Velázquez,[1] G. Georgiou,[2] M. Sentmanat,[3] S.G. Hatzikiriakos[1]
[1] *Department of Chemical and Biological Engineering, The University of British Columbia, Vancouver, British Columbia, Canada*

[2] *Department of Mathematics and Statistics, University of Cyprus, Nicosia, Cyprus*

[3] *Xpansion Instruments, LLC, Tallmadge, Ohio*

The sharkskin and stick-slip polymer extrusion instabilities are studied primarily as functions of the type of die geometry. Experimental observations concerning the flow curves, the critical wall shear stress for the onset of the instabilities, the pressure and flow rate oscillations, and the effects of geometry and operating conditions are presented for linear low-density polyethylenes. It is found that sharkskin and stick-slip instabilities are present in the capillary and slit extrusion. However, annular extrusion stick-slip and sharkskin are absent at high ratios of the inside-to-outside diameter of the annular die. This observation also explains the absence of these phenomena in other polymer processing operations such as film blowing. These phenomena are explained in terms of the surface-to-volume ratio of the extrudates, that is, if this ratio is high, sharkskin and stick-slip are absent. **POLYM. ENG. SCI., 48:405–414, 2008. © 2007 Society of Plastics Engineers**

INTRODUCTION

The instabilities that occur in the extrusion of molten polymers are fascinating from the scientific perspective, but troublesome and frequently catastrophic from the industrial one [1]. Over the past 50 years, there has been sustained interest in the understanding and control of these instabilities [2]. They can occur in common extrusion operations such as in the manufacture of polymeric rods, tubes, sheets, profiles, films, and wire coating.

Since its onset occurs at relatively low rates of production, sharkskin which is characterized by small amplitude periodic surface distortions is the most troublesome of these instabilities and is often one of the first processing-related issues to be addressed in extrusion [3]. Two frequently cited contributions from the 80s are the articles by Ramamurthy [1] and Kalika and Denn [4], who studied the sharkskin of linear low-density polyethylenes (LLDPEs) and the effects of different die materials. Subsequently, El Kissi and Piau [5, 6] studied extensively the extrusion instabilities for moderately and highly entangled polydimethylsiloxanes, LLDPEs and polybutadienes (PBs).

Stick-slip flow is a processing instability that is characterized by pressure and flow rate oscillations during controlled throughput extrusion and manifested by periodic, alternating rough and smooth regions on the surface of the extrudate [7]. The stick-slip instability has been the subject of experimental studies since the late 1950s and has been given many different names such as stick-slip, cyclic, bamboo, cork flow, and oscillating melt fracture by researchers studying polymer extrusion instabilities [7, 8]. Systematic observations on the oscillating melt fracture behavior of high density polyethylenes (HDPEs) have been reported by Lupton and Regester [9] and Myerholtz [10]. Vinogradov and coworkers [11–13] investigated thoroughly the flow of narrow molecular-weight-distribution polyisoprenes and PBs in both pressure- and flow-rate-controlled experiments, and introduced the term *spurt flow* for the stick-slip. In the early 1990s, Hatzikiriakos and Dealy [14] studied the stick-slip of HDPEs, for which they used the term *cyclic melt fracture*. Important contributions on the origin of this instability were made by Wang and Drda [15–17], who studied systematically the extrusion of linear PE melts and the molecular origins of the stick-slip instability. Recent work on the subject concerns the use of direct pressure drop measurements and their relation with local velocity distributions [18–20]. Recent publications discuss thoroughly the origin of this type of flow and provide important literature reviews [21–22].

Correspondence to: S.G. Hatzikiriakos; e-mail: hatzikir@interchange.ubc.ca
Contract grant sponsors: NSERC; CONACyT.
DOI 10.1002/pen.20939
Published online in Wiley InterScience (www.interscience.wiley.com).
© 2007 Society of Plastics Engineers

WILEY InterScience® DISCOVER SOMETHING GREAT

Most of the experimental studies cited earlier involved extrusion through capillary dies, with the exception of those studies incorporating the use of local velocity measurements [18–20] which involved extrusion through orthogonal channels. To date, few observations have been reported in the literature on the occurrence of oscillating melt fracture and sharkskin melt fracture involving extrusion through annular dies. Since many common polymer processing operations such as film blowing, blow molding, wire coating, pipe extrusion, and specialty profile extrusion operations involve extrusion through annular dies, an experimental study identifying the conditions under which sharkskin and oscillating melt fracture occur during annular die flow would be of great practical importance. Rosenbaum [23] and Rosenbaum et al. [24] have reported experimental data for a linear metallocene PE in capillary extrusion and identified clearly the occurrence of stick-slip instability. However, their data for a crosshead die (annular die) showed a continuous flow curve with no hint of stick-slip. Moreover, the reported critical shear rate for the onset of sharkskin melt fracture was much higher than that obtained in capillary extrusion. It is the objective of this work to study systematically this phenomenon by using several capillary, slit, and annular dies. Moreover, an attempt will be made to identify the origin of this different behavior of linear polymers in capillary, slit, and annular dies with regard to sharkskin and stick-slip instabilities. In addition, this study can be used as a guide for assessing the processability of polymers using a capillary/slit/annular rheometer and inferring their processing behavior in industrial applications.

MATERIALS AND METHODOLOGY

The LLDPE resin used in this study was a Ziegler-Natta, hexane copolymer supplied by ExxonMobil (LL3001). It has a melt index of about 1 at 190°C, a density of 0.917 at 25°C, and a zero shear viscosity of 24.56 kPa s at 150°C.

Parallel plate rheometry was performed to determine the linear viscoelastic properties of the LLDPE resin at several temperatures. The measurements were performed using a Rheometrics System IV (controlled-strain) and a Bohlin-CVOR (controlled-stress rheometer). Experiments were performed at different temperatures, namely 130, 150, 170, 190, and 210°C. Mastercurves were obtained, and the most results are presented at the reference temperature of 150°C.

The extensional rheological characterization of the LLDPE was performed using an SER Universal Testing Platform [25, 26] from Xpansion Instruments. As described by Sentmanat [25, 26], the SER unit is a dual windup extensional rheometer that has been specifically designed for use as a fixture on a variety of commercially available rotational rheometer host platforms. The particular SER model used in this study, a model SER-HV-B01, was designed for use on a VOR Bohlin rotational rheometer host system. Specimens were prepared by compression molding the polymer samples between polyester films to a gage of about 1 mm, at 20 MPa and 170°C, using a hydraulic press. Individual polymer specimens were then cut to a width of 6.4–12.7 mm. Typical SER extensional melt rheology specimens range from 40 to 150 mg in mass. Measurements were conducted at the shear rheology mastercurve reference temperature of 150°C, more than 25° above the peak melting point of the polymer.

Extrusion experiments in a capillary rheometer using various dies were used to assess the processability of the LLDPE and the critical parameters for the onset of flow instabilities such as sharkskin and oscillating melt fracture. Table 1 summarizes the dimensions of the dies corresponding to the different geometries used in this study. First, capillary extrusion measurements were conducted at 150 and 190°C using three different capillary dies having diameters, D, equal to 0.43, 0.762, and 2.34 mm; and a length-to-diameter ratio, L/D, from 14 to 16. The onset of oscillating melt fracture was determined from the pressure signal as well as from the alternate relatively smooth and distorted sections along the extrudates using an Olympus MIC-D microscope. The same microscope was used to detect sharkskin melt fracture.

Second, similar experiments were performed with three slit dies having different height, H, width, W, length-to-height ratios, L/H, and entrance angles, 2α, of 180° for two dies, and 60° for the other one. The aspect ratio of their cross sections was near 10, and thus the calculated shear stress based on a typical analysis of slit flow to produce rheological data is valid [27].

Finally, three annular dies were used to determine the flow curve of the LLDPE in annular flow using different inside-to-outside diameter ratios, D_i/D_o, ranging from

TABLE 1. Different die geometries used in this study along with their dimensions.

Capillary		
D (mm)	L/D	2α (°)
0.432	15	180
0.762	16	180
2.34	14	180

Slit die			
H (mm)	W (mm)	L/H	2α (°)
0.305	2.6	34	180
0.324	2.45	31	60
0.47	2.54	44	180

Tube extrusion				
RR	D_o (mm)	D_i (mm)	D_i/D_o	$L/(D_o - D_i)$
152	2.54	1.542	0.607	10
350	2.54	2.167	0.853	27
1000	2.54	2.415	0.951	80

DOI 10.1002/pen

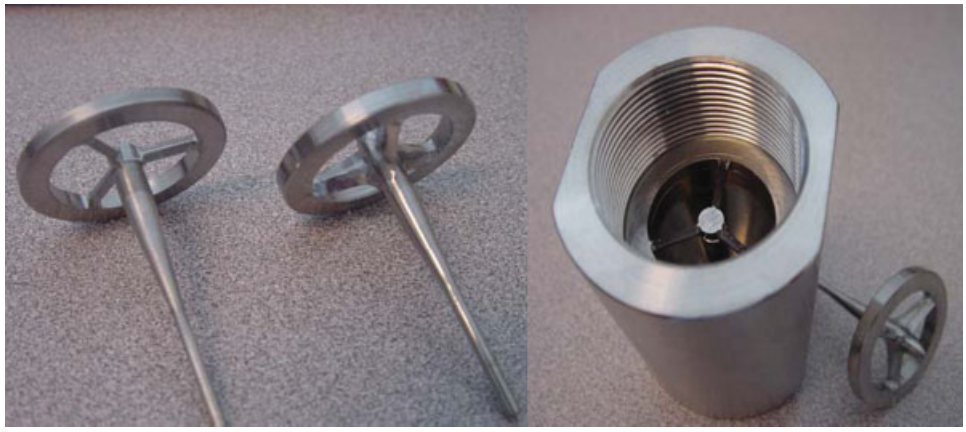

FIG. 1. A picture of the annular die showing the various inserts that are used to change the gap. [Color figure can be viewed in the online issue, which is available at www.interscience.wiley.com.]

0.607 to 0.951 (see Table 1 for details), with reduction ratios RR (ratio of cross-sectional areas), equal to 152, 350, and 1000, correspondingly. It is noted that an annular die having a D_i/D_o ratio approaching zero becomes similar to a capillary die, whereas a D_i/D_o approaching 1 becomes similar to a slit die. A picture of a typical annular die appears in Fig. 1, where the different inside pieces are also shown.

RESULTS AND DISCUSSION

Linear Viscoelastic Measurements

The linear viscoelastic behavior of pure LLDPE was studied in detail over the temperature range of 130–210°C, as discussed earlier. Time-temperature superposition was applied to shift the data horizontally in order to obtain a mastercurve at a reference temperature, $T_{ref} = 150$°C. Horizontal shift factors, a_T, which reflect temperature dependence of relaxation time, were obtained following the procedure proposed by Mavridis and Shroff [28], where a_T is described by an Arrhenius equation, as follows:

$$\log(a_T) = \frac{E_a}{R}\left(\frac{1}{T} - \frac{1}{T_{ref}}\right), \quad (1)$$

where E_a is the "horizontal activation energy" and R is the universal gas constant.

Figure 2 shows the master storage modulus, G', and loss modulus, G'', as well the master complex viscosity, η^*/a_T, versus reduced frequency, $\alpha_T\omega$ for the pure LLDPE. The superposition is satisfactory, typical for linear polymers. The resulting energy of activation was about 8 kcal/mol that is typical for a LLDPE, as reported by Mavridis and Shroff [28] and Hatzikiriakos [29].

Extensional Measurements

Extensional rheological measurements were conducted at 150°C for the pure LLDPE. The extensional rheological behavior of pure resin is depicted in Fig. 3. The tensile stress growth coefficients, η_E^+, are plotted for three different Hencky strain rates, namely 0.1, 1, and 10 s^{-1} as functions of time. It can be observed that LLDPE

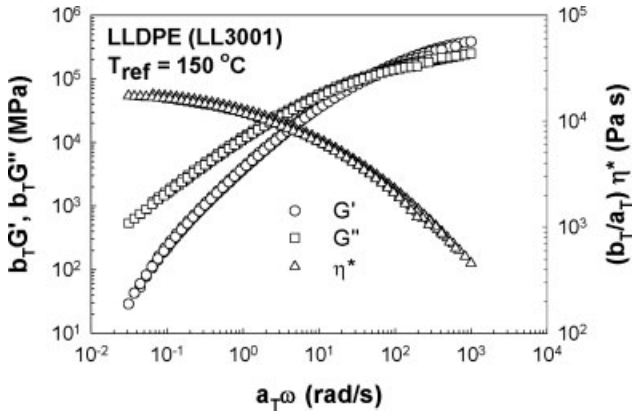

FIG. 2. The master viscoelastic moduli and complex viscosity of LLDPE (LL3001) at 150°C.

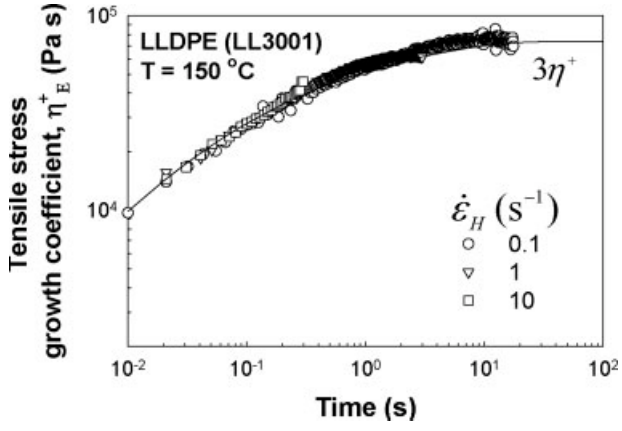

FIG. 3. The tensile stress growth coefficient curves for the LLDPE resin (LL3001) at three different Hencky strain rates: 0.1, 1, and 10 s^{-1}; at 150°C. The absence of strain hardening is typical for a linear polymer.

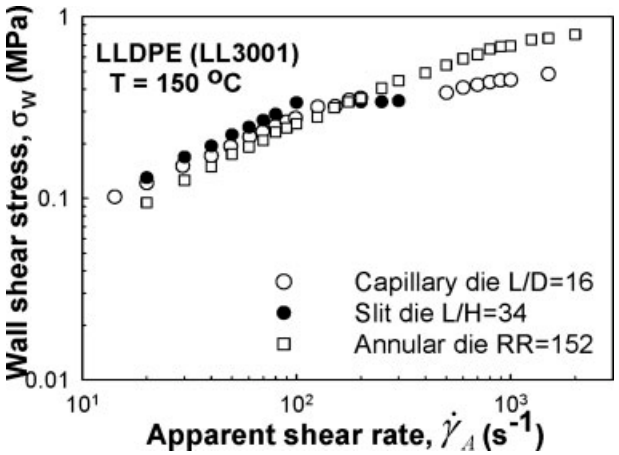

FIG. 4. Typical flow curves of LLDPE in capillary, slit, and annular extrusion at 150°C.

(LL3001) does not exhibit any degree of strain hardening at any extension rate, an observation consistent with polymers of linear architecture. In addition, the tensile stress growth curves display very little deviation from the linear viscoelastic envelope, $3\eta^+$, that was determined independently from linear viscoelastic shear rheology measurements, plotted as a continuous line in Fig. 3, an indication of the consistency of the experimental data.

Flow Curves

Plots of wall shear stress versus apparent shear rate, known as flow curves, at 150°C are depicted in Fig. 4 using three different geometries; namely, a capillary die ($D = 0.762$ cm, $L/D = 16$), slit die ($H = 0.305$ mm, $L/H = 34$), and tube extrusion die ($D_i/D_o = 0.607$, $RR = 152$). For shear rates below 100 s^{-1}, the flow curve for the slit die lies above those obtained with the other die

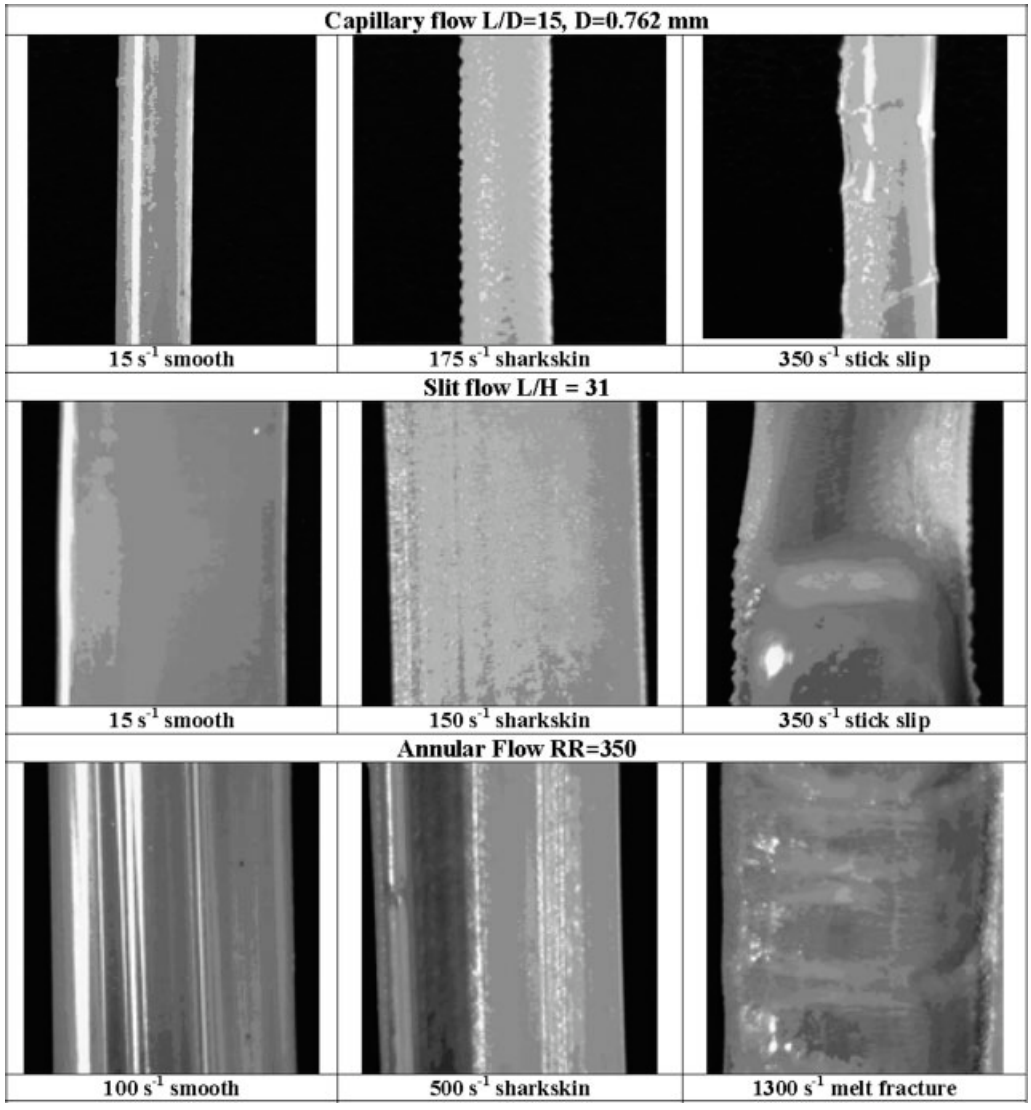

FIG. 5. Photographs of extrudates from capillary, slit, and annular extrusion experiments at 150°C.

 DOI 10.1002/pen

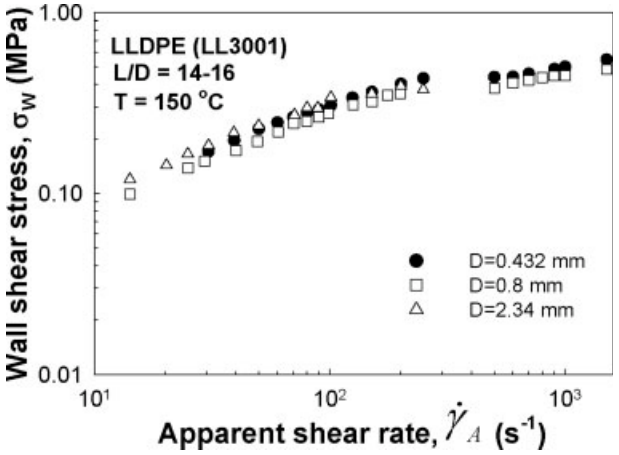

FIG. 6. Flow curves of LLDPE in capillary extrusion at 150°C for three different capillary dies with $L/D = 14$–16 and diameters ranging from 0.43 to 2.34 mm. The discontinuities indicate the presence of stick-slip flow.

geometries. This is mainly because the wall shear stress was calculated without measuring the Bagley correction. Moreover, an additional error in slit rheometry originates from the finite aspect ratio of the die.

Discontinuities in the flow curves can be observed for capillary and slit flow, which are mainly due to the occurrence of oscillating flow (stick-slip flow); however, in the case of annular extrusion, there are no discontinuities, and thus no stick-slip has been observed. As will be discussed later, this is the case with all three-tube extrusion dies.

Figure 5 shows typical photographs of the extrudates taken from the three different geometries used in this study. Extrudate pictures of samples collected during extrusion in the smooth, sharkskin, and stick-slip melt fractures flow regimes can be seen, depending on the individual cases.

Capillary Flow

Figure 6 shows the flow curves of LLDPE obtained in capillary flow at 150°C using all three capillary dies. The critical shear rates and wall shear stresses for the onset of sharkskin and oscillating melt fracture are listed in Tables 2 and 3. First, at 150°C, the critical shear stress for the onset of sharkskin is in the range of 0.17–0.19 MPa, consistent with values reported previously in the literature [1]. Discontinuities in the flow curves, which define the stick-slip flow regime, were observed only for the dies having smaller diameters, i.e., 0.432 and 0.762 mm; for the larger diameter die, this flow regime should appear at higher apparent shear rates not accessible with our capillary rheometer. Furthermore, the onset of these discontinuities with the smaller diameter capillaries were obtained at apparent shear rate values of 300 and 230 s^{-1}, respectively, and shear stress oscillations of 0.31–0.40 and 0.43–0.44 MPa, respectively (see Table 2). The amplitude of these oscillations depends on the diameter of the die [14].

At 190°C, stick-slip was also present in the dies with 0.432 mm and 0.762 mm diameter, as observed from the discontinuity on the flow curves on Fig. 7. In both cases, the onset of the oscillations is shifted to higher apparent shear rates (600 and 850 s^{-1}) with respect to the flow curves at 150°C. Typical pressure oscillations obtained with the die having a diameter of 0.762 mm are shown in Figs. 8 and 9, at 150 and 190°C, respectively. Moreover, for all the three capillary dies, the onset of sharkskin melt fracture is shifted to higher shear rates when the temperature is increased from 150 to 190°C.

Slit Flow

The flow curves for slit flow for LLDPE at 150°C using the three different slit dies are shown in Fig. 10. Sharkskin and stick-slip is present in all cases; the critical shear stresses for the onset of sharkskin are in the range 0.16–0.22 MPa and, in general, much higher than the corresponding ones in capillary extrusion. The critical apparent shear rates and stresses for the onset of instabilities are listed in Tables 4 and 5.

Figure 11 depicts the flow curves for LLDPE in slit extrusion at 190°C. Stick-slip is also present in the three-slit die geometries; however, the critical shear rates for its onset are smaller than those obtained at 150°C. In general, the critical shear stresses for the onset of sharkskin are again higher (0.12–0.25 MPa) than the corresponding values obtained in capillary extrusion (0.15–0.17 MPa).

Typical pressure oscillations obtained with the slit die having a height of 0.305 mm are shown in Figs. 12 and 13, at 150 and 190°C, respectively.

TABLE 2. Critical shear rates and stresses for LLDPE (LL3001) in capillary flow at 150°C.

	Sharkskin MF		Stick-slip	
D (mm)	σ_W (MPa)	$\dot{\gamma}_A$ (s^{-1})	σ_W (MPa)	$\dot{\gamma}_A$ (s^{-1})
0.432	0.19	30	0.43–0.44	300
0.80	0.19	50	0.31–0.40	230
2.34	0.17	25	—	Not accessed

TABLE 3. Critical shear rates and stresses for LLDPE (LL3001) in capillary flow at 190°C.

	Sharkskin MF		Stick-slip	
D (mm)	σ_W (MPa)	$\dot{\gamma}_A$ (s^{-1})	σ_W (MPa)	$\dot{\gamma}_A$ (s^{-1})
0.432	0.16	70	0.40–0.41	600
0.80	0.17	90	0.39–0.42	850
2.34	0.15	50	—	Not accessed

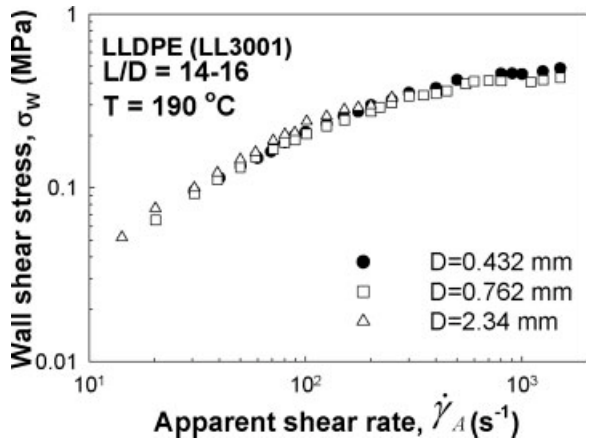

FIG. 7. Flow curves of LLDPE in capillary extrusion at 190°C for three different capillary dies with $L/D = 14$–16 and diameters ranging from 0.43 to 2.34 mm. Discontinuities appear in all cases (identified by a plateau in the data), indicating the presence of stick-slip flow.

Annular Flow

For the case of annular flow, the flow curves at 150 and 190°C, using all the available annular dies are depicted in Figs. 14 and 15 respectively. No stick-slip flow regime was observed, at any temperature, as can be observed by the monotonous increase of wall shear stress versus apparent shear rate relationships.

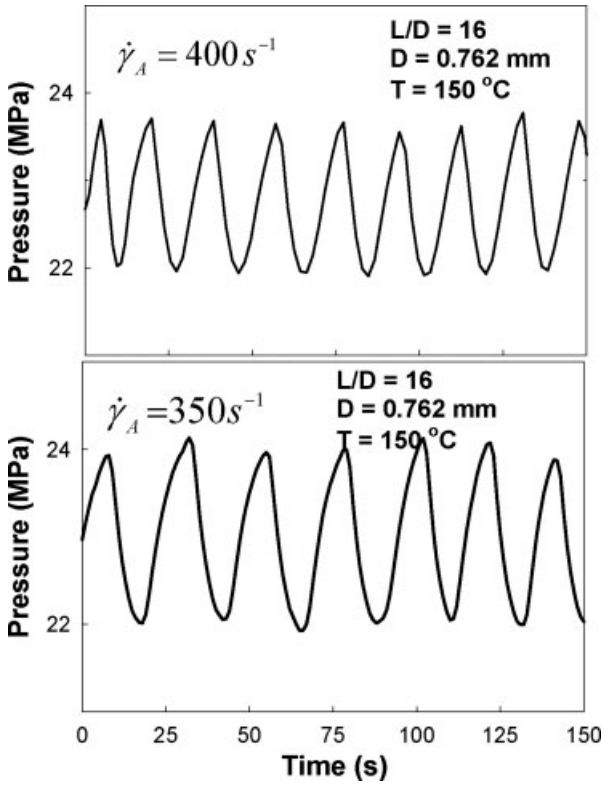

FIG. 8. Typical pressure oscillations in capillary flow using a die having $D = 0.762$ mm, $L/D = 16$ at various apparent shear rates and at 150°C.

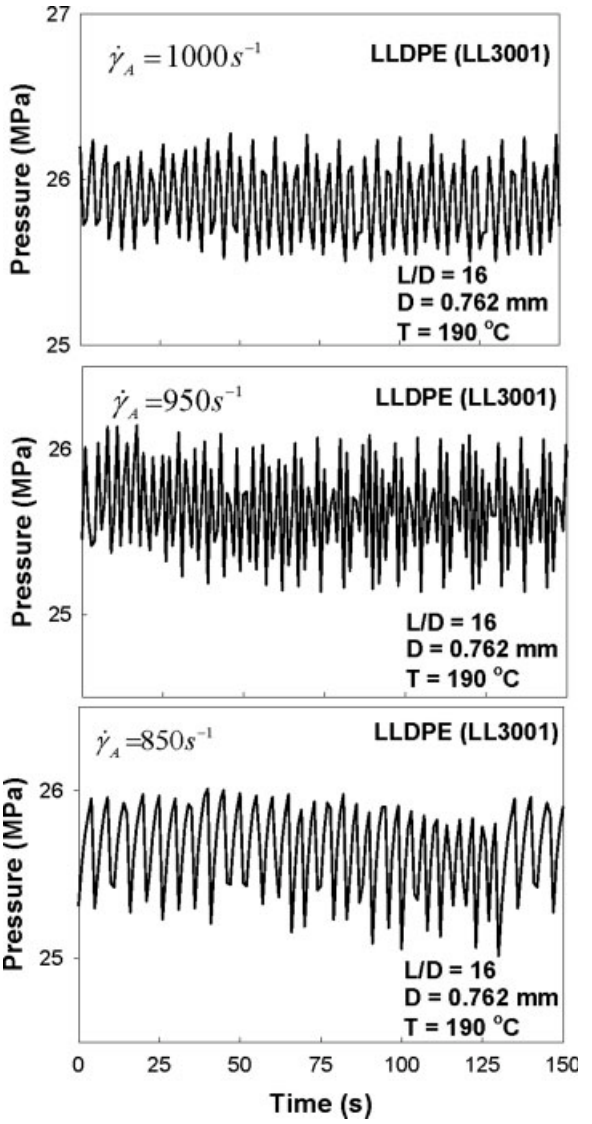

FIG. 9. Typical pressure oscillations in capillary flow using a die having $D = 0.762$ mm, $L/D = 16$ at various apparent shear rates and at 190°C.

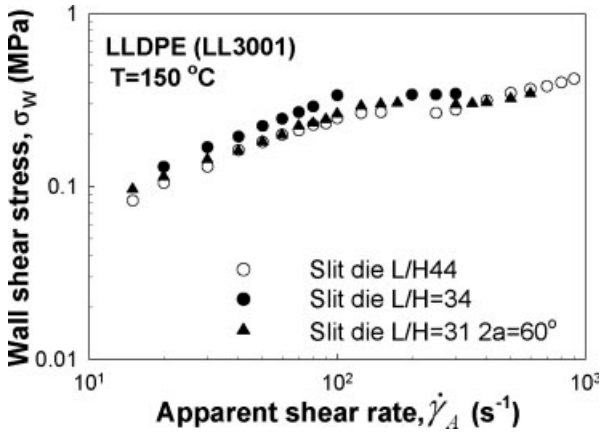

FIG. 10. Flow curves of LLDPE in slit die extrusion at 150°C using the three different slit dies. Discontinuities appear in all cases indicating the presence of stick-slip (oscillating) flow.

DOI 10.1002/pen

TABLE 4. Critical shear rates and stresses for LLDPE (LL3001) in slit flow at 150°C.

	Sharkskin MF		Stick-slip	
L/H	σ_W (MPa)	$\dot{\gamma}_A$ (s^{-1})	σ_W (MPa)	$\dot{\gamma}_A$ (s^{-1})
34	0.20	60	0.38–0.32	150
44	0.17	40	0.28–0.26	175
31	0.22	70	0.34–0.29	200

Regarding the onset of sharkskin melt fracture, Tables 6 and 7 summarize the critical shear rates and wall shear stresses for the onset of this instability for the three annular dies. At the higher temperature, only for the smallest reduction ratio (RR = 152) that corresponds to higher annular gap of $D_i/D_o = 0.607$, sharkskin was observed. At 150°C the critical shear stress values increased with D_i/D_o from 0.36 MPa to about 1 MPa. These values and the corresponding apparent shear rate values are much higher than the corresponding critical values obtained in capillary and slit extrusion.

DISCUSSION

In our experimental study, it was found that LLDPE exhibits sharkskin through capillary, slit, and annular dies. However, it was found that the melt undergoes sharkskin in annular dies at considerably higher shear rates compared to those in slit dies, and these in turn are higher than the ones obtained in capillary extrusion. As has been described in earlier studies [3, 30–33], the onset of sharkskin is believed to be due to a localized melt rupture phenomenon initiated at the free surface of the extrudate and propagated inward upon exiting the die. The singularity that occurs at the die exit as the melt abruptly transitions from a fixed boundary to free surface results in high extensional flow deformations isolated to the region of the melt nearest the outermost layer of the extrudate. The periodicity of the sharkskin melt fracture comes as a result of the intermittent elastic energy storage via tensile modulus increase and elastic energy dissipation via transverse crack propagation along the surface region of the extrudate. Although highly branched materials have an inherent means of rapidly dissipating this

TABLE 5. Critical shear rates and stresses for LLDPE (LL3001) in slit flow at 190°C.

	Sharkskin MF		Stick-slip	
L/H	σ_W (MPa)	$\dot{\gamma}_A$ (s^{-1})	σ_W (MPa)	$\dot{\gamma}_A$ (s^{-1})
34	0.25	150	0.33–0.34	300
44	0.12	40	0.33–0.34	550
31	0.21	125	0.38–0.39	700

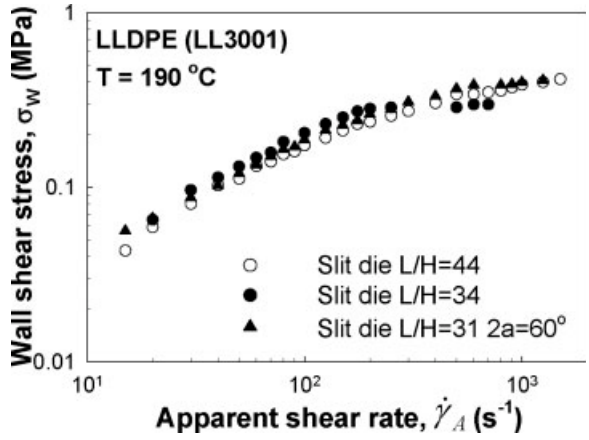

FIG. 11. Flow curves of LLDPE in slit die extrusion at 190°C using the three slit dies. Discontinuities appear in all cases (identified by a plateau in the data), indicating the presence of stick-slip flow.

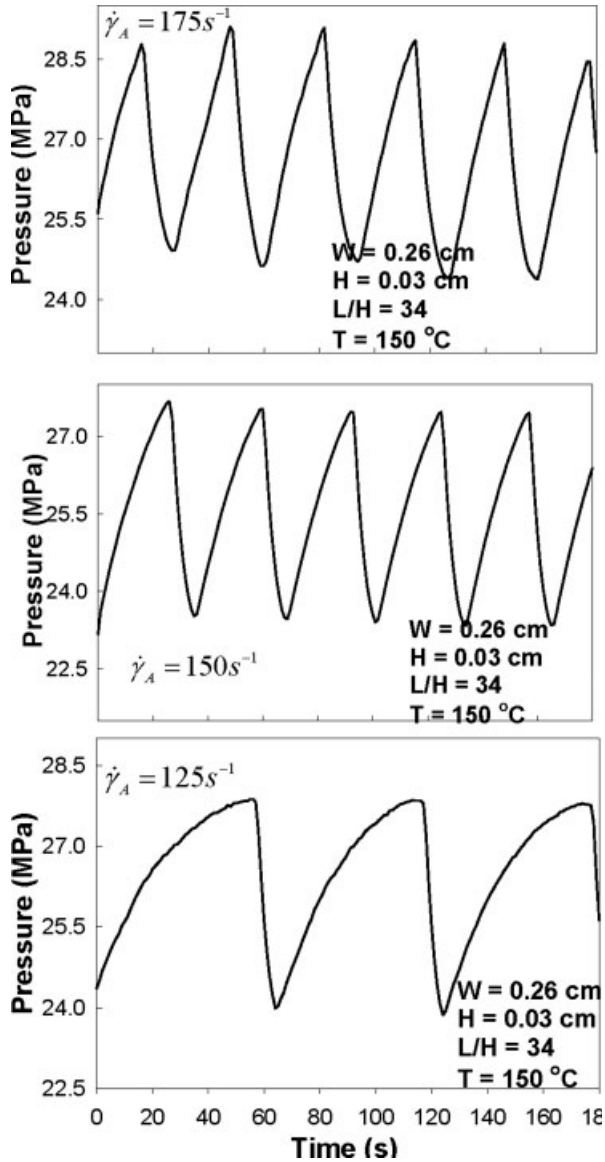

FIG. 12. Typical pressure oscillations in slit flow at 150°C.

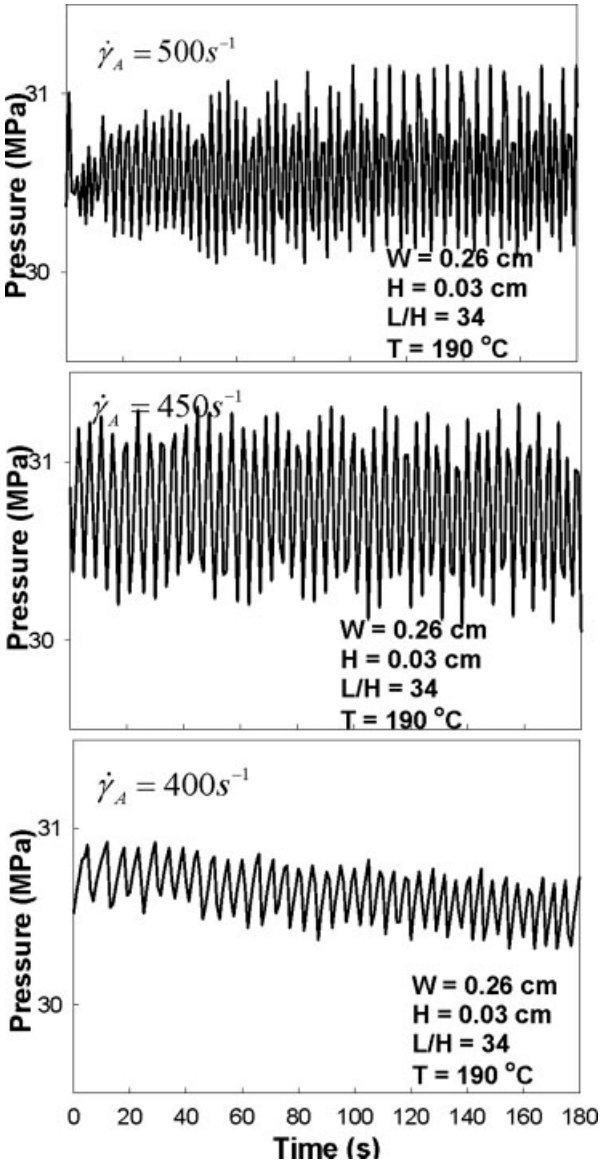

FIG. 13. Typical pressure oscillations in slit flow at 190°C.

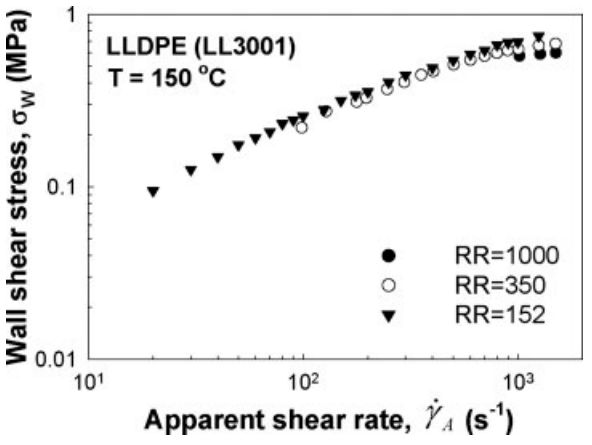

FIG. 14. Flow curves of LLDPE in annular extrusion at 150°C using three reduction ratios: RR = 152, 350, and 1000; no discontinuity has been observed.

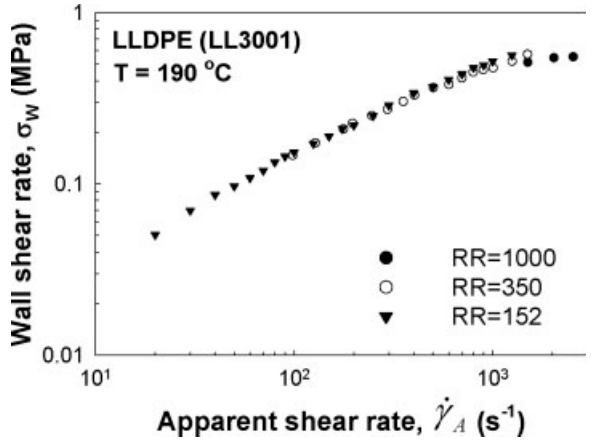

FIG. 15. Flow curves in annular extrusion at 190°C using three reduction ratios: RR = 152, 350, and 1000; no discontinuity has been observed.

free surface stress condition, viz branch mobility (in which the lower molecular weight branches are able to rapidly reconfigure themselves toward a lower stress state condition while the large molecular backbone hardly participates in this rapid energy dissipation process), linear materials must dissipate this stress by only one means—along their large molecular backbone. Consequently, linear polyethylenes are prone to this type of sharkskin melt fracture phenomenon due to the fact that, at high extensional flow rates, they exhibit both a rapid increase in elastic tensile modulus and a brittle-type mode of failure at rupture, factors that inherently contribute to crack propagation [33, 34]. Slip promoters also alleviate this critical stress condition at the free surface by reducing the extensional deformation witnessed by the material at the extrudate surface immediately upon exiting the die [3]. Hence with sharkskin, the critical factor in determining the onset of melt fracture is how rapidly the material at the free surface of the extrudate can dissipate energy and assume a lower stress state configuration at the free surface.

It is believed that the primary reason that the annular extrusion die yields a delayed onset for sharkskin melt fracture lies in the fact that the material exiting the die has the largest surface area-to-volume aspect ratio at the die exit. This increased surface area ratio coupled with

TABLE 6. Critical shear rates and stresses for LLDPE (LL3001) in annular flow at 150°C.

	Sharkskin MF		Stick-slip	
RR	σ_W (MPa)	$\dot{\gamma}_A$ (s^{-1})	σ_W (MPa)	$\dot{\gamma}_A$ (s^{-1})
152	0.36	200	–	—
350	0.47	400	—	—
1000	1	150	—	—

DOI 10.1002/pen

TABLE 7. Critical shear rates and stresses for LLDPE (LL3001) in annular flow at 150°C.

	Sharkskin MF		Stick-slip	
RR	σ_W (MPa)	$\dot{\gamma}_A$ (s^{-1})	σ_W (MPa)	$\dot{\gamma}_A$ (s^{-1})
152	0.37	500	—	—
350	—	—	—	—
1000	—	—	—	—

the fact that an annulus has no edges allows the material at the free surfaces additional degrees of freedom to rapidly assume a lower stress state as it exits the die. Unlike a slit that is confined by its edges, an annular geometry can allow for a subtle spiraling flow (three-dimensional flow) as it exits the die, thereby benefiting from an additional degree of freedom than material exiting a slit die, where the flow over a majority of the web is primarily a 2D flow. Although a capillary die can also allow for spiraling flow, it has the lowest surface area-to-volume ratio of the three geometries and only a single free surface over which a lower stress state configuration must be rapidly achieved upon exiting the die. One can think of this as a critical surface stress condition per unit surface area that must be achieved for sharkskin to occur. Hence, the increased free surface area and ability to allow for 3D flow enable materials extruded from an annular die to exhibit a delayed onset to sharkskin melt fracture when compared to capillary and slit die geometries.

Furthermore, it is believed that the lack of an observable stick-slip flow regime with annular die flow is due to an inherent difference in the converging flow section in the entrance region of the die when compared to the slit and capillary die geometries. Because of the presence of the central mandrel support in the entrance region of the annular die, the vortex-like flow in the die entrance region that would otherwise accompany the onset of the stick-slip instability is inherently stifled.

CONCLUSIONS

The sharkskin and oscillatory melt fracture behavior of a LLDPE was studied at two different temperatures, 150 and 190°C in capillary, slit, and annular flows. Oscillatory melt fracture was observed only in capillary and slit flows. In both cases, the onset of the pressure oscillations is shifted to higher apparent shear rates as the temperature is increased from 150 to 190°C. As for the annular flow, three different reduction ratios (RR) were used: 152, 350, and 1000. There were no oscillations present in any of the three dies and temperatures. In addition, it was observed that the critical shear rate and stress for the onset of sharkskin in annular flow is considerably higher than those detected in slit extrusion and those higher than the ones determined in capillary flow. These results were explained in terms of a critical surface stress condition per unit surface area that must be achieved for sharkskin to occur. It was also argued that the annular flow allows for a 3D spiraling flow that provides additional degrees of freedom for the stress concentration at the exit to be relieved. Finally, the lack of an observable stick-slip flow regime with annular die flow is due to an inherent difference in the converging flow section in the entrance region of the die when compared to the slit and capillary die geometries.

REFERENCES

1. A.V. Ramamurthy, *J. Rheol.*, **30**, 337 (1986).
2. S.G. Hatzikiriakos and K.B. Migler, Eds., *Polymer Processing Instabilities: Control and Understanding*, Marcel Dekker, New York (2005).
3. K.B. Migler, "Sharkskin Instability in Extrusion," in *Polymer Processing Instabilities: Control and Understanding*, S.G. Hatzikiriakos and K.B. Migler, Eds., Marcel Dekker, New York, 121 (2005).
4. D.S. Kalika and M.M. Denn, *J. Rheol.*, **31**, 815 (1987).
5. N. El-Kissi and J.M. Piau, *C.R. Acad. Sci. Paris*, **309(Série II)**, 7 (1989).
6. N. El-Kissi and J.M. Piau, *J. Non-Newtonian Fluid Mech.*, **37**, 55 (1990).
7. J.P. Tordella, *J. Appl. Phys.*, **27**, 454 (1956).
8. E.B. Bagley, I.M. Cabott, and D.C. West, *J. Appl. Phys.*, **29**, 109 (1958).
9. J.M. Lupton and J.W. Regester, *Polym. Eng. Sci.*, **5**, 235, (1965).
10. R.W. Myerholtz, *J. Appl. Polym. Sci.*, **11**, 687 (1967).
11. G.V. Vinogradov, M.L. Driedman, N.V. Yarlykov, and A.Y. Malkin, *Rheol. Acta*, **9**, 323 (1970).
12. G.V. Vinogradov, A.Y. Malkin, Y.G. Yanovskii, E.K. Borisenkova, B.V. Yarlykov, and G.V. Berezhnaya, *J. Polym. Sci. Part A-2 Polym. Phys.*, **10**, 1061 (1972).
13. G.V. Vinogradov, V.P. Protasov, and V.E. Breval, *Rheol. Acta*, **23**, 46 (1984).
14. S.G. Hatzikiriakos and J.M. Dealy, *J. Rheol.*, **36**, 845 (1992).
15. S.Q. Wang and P.A. Drda, *Macromolecules*, **29**, 2627 (1996).
16. S.Q. Wang and P.A. Drda, *Macromolecules*, **29**, 4115 (1996).
17. S.Q. Wang and P.A. Drda, *Rheol. Acta*, **36**, 128 (1997).
18. H. Münstedt, M. Schmidt, and E. Wassner, *J. Rheol.*, **44**, 413 (2000).
19. L. Robert, B. Vergnes, and Y. Demay, *Proc. 6th Eur. Conf. Rheol.*, Erlangen, 145 (2002).
20. A. Merten, M. Schwets, and H. Münstedt, *Proc. 6th Eur. Conf. Rheol.*, Erlangen, **147** (2002).
21. G. Georgiou, "Stick-Slip Instability," in *Polymer Processing Instabilities: Control and Understanding*, S.G. Hatzikiriakos

and K.B. Migler, Eds., Marcel Dekker, New York (2005).
22. M.A. Ya, *Polym. Sci. Ser. C*, **48**, 21 (2006).
23. E.E. Rosenbaum, "Rheology and Processability of FEP Teflon Resins for Wire Coating," PhD Thesis, University of British Columbia (1998).
24. E.E. Rosenbaum, S. Randa, S.G. Hatzikiriakos, and C.W. Stewart, *Polym. Eng. Sci.*, **40**, 179 (2000).
25. M. Sentmanat, U.S. Patent No. 6,578,413 (2003).
26. M. Sentmanat, *Rheol. Acta*, **43**, 657 (2004)
27. J.M. Dealy and K.F. Wissbrun, *Melt Rheology and its Role in Plastics Processing: Theory and Applications*, Van Nostrand Reinhold, New York (1990).
28. H. Mavridis and R.N. Shroff, *Polym. Eng. Sci.*, **32**, 1778 (1992).
29. S.G. Hatzikiriakos, *Polym. Eng. Sci.*, **40**, 2279 (2000).
30. F.N. Cogswell, *J. Non-Newtonian Fluid Mech.*, **2**, 37 (1977).
31. K.B. Migler, Y. Son, F. Qiao, and K. Flynn, *J. Rheol.*, **46**, 383 (2002).
32. M. Sentmanat and S.G. Hatzikiriakos, *Rheol. Acta.*, **43**, 624 (2004).
33. M. Sentmanat, E.B. Muliawan, and S.G. Hatzikiriakos, *Rheol. Acta*, **44**, 1 (2005).
34. E.B. Muliawan, S.G. Hatzikiriakos, and M. Sentmanat, *Int. Polym. Process.*, **XX**, 60 (2005).

 DOI 10.1002/pen